Cellular and Molecular Life Sciences (2025) 82:132
https://doi.org/10.1007/s00018-025-05653-5

ORIGINAL ARTICLE

METTL3-dependent m6A methylation of circCEACAM5 fuels pancreatic cancer progression through DKC1 activation

Jie Zhang[1] · Wenxue Sun[2] · Wenda Wu[3] · Zihui Qin[3] · Ben Wei[3] · Tushuai Li[1]

Received: 14 November 2024 / Revised: 20 February 2025 / Accepted: 7 March 2025

Abstract

Background Pancreatic cancer is highly lethal and has a poor prognosis. Research has highlighted the role of circular RNAs and m6A methylation in cancer progression. METTL3, a key m6A methyltransferase, is linked to various cancers, but its interaction with circular RNAs in pancreatic cancer is unclear. This study examined the role of circCEACAM5 in pancreatic cancer, particularly its regulation by METTL3-mediated m6A methylation and interaction with effectors such as DKC1.

Methods circCEACAM5 expression in pancreatic cancer tissues and cell lines was evaluated via RT−qPCR. Its characteristics were validated through Sanger sequencing, stability assays, and FISH. Functional assays (CCK-8, EdU, Transwell, and flow cytometry) were conducted in AsPC-1 cells, and in vivo tumor models were established. m6A modification was analyzed via bioinformatics tools and m6A-specific immunoprecipitation, while RNA pull-down assays were used to examine the interaction of circCEACAM5 with METTL3 and DKC1.

Results circCEACAM5 was significantly upregulated in pancreatic cancer and correlated with poor clinical outcomes. CircCEACAM5 promoted cell proliferation, invasion, and migration while inhibiting apoptosis both in vitro and in vivo. METTL3-mediated m6A methylation of circCEACAM5 was confirmed, and METTL3 knockdown reversed the effects of circCEACAM5 silencing on the malignant behavior of pancreatic cancer cells. circCEACAM5 interacted with DKC1, and DKC1 overexpression reversed the effects of circCEACAM5 knockdown on the malignant behavior of pancreatic cancer cells.

Conclusion METTL3-mediated m6A methylation of circCEACAM5 drives pancreatic cancer progression by increasing DKC1 expression, suggesting potential new therapeutic targets for this aggressive malignancy.

Keywords Pancreatic cancer · M6A methylation · CircCEACAM5 · METTL3 · DKC1

Background

Pancreatic cancer is a serious malignancy of the digestive system that ranks third in terms of cancer-related deaths [1]. The incidence of pancreatic cancer is increasing annually, and it is likely to be the second most common tumor by 2030 [2], causing a considerable burden on global health and economies. The onset of pancreatic cancer is insidious; only 15%−20% of patients with pancreatic cancer are eligible for radical surgery, and the 5-year survival rate is less than 9% [3]. Because pancreatic cancer is prone to early metastasis, it is not sensitive to traditional radiotherapy and chemotherapy, and the treatment methods are limited, so the mortality rate is high. Therefore, studying the pathogenesis of pancreatic cancer is crucial for the development of new treatments [4].

Over the past decade, circular RNAs (circRNAs), a major class of noncoding RNA molecules, have played key roles in the onset and progression of cancer through different mechanisms of action [5]. CircRNAs are closed circular transcripts formed via alternative splicing of precursor mRNAs [6]. CircRNAs are highly abundant, highly stable, sequentially conserved, and specific to tissues and cells, indicating that they play important regulatory roles in the occurrence and progression of disease [7]. Scholars have reported that circRNAs are significantly differentially expressed in diseases

✉ Tushuai Li
litushuai@cslg.edu.cn

[1] School of Biology and Food Engineering, Changshu Institute of Technology, Suzhou 215500, People's Republic of China

[2] Jining First People's Hospital, Jining Medical University, Jining 272000, People's Republic of China

[3] MOE Joint International Research Laboratory of Animal Health and Food Safety, College of Veterinary Medicine, Nanjing Agricultural University, Nanjing 210095, People's Republic of China

Published online: 27 March 2025

such as tumors, cardiovascular diseases, and neurological diseases. With the deepening of pancreatic cancer research, circRNAs have been confirmed to be involved in multiple biological processes of pancreatic cancer [8]. For example, circPDE8A facilitates pancreatic cancer cell growth through the miR-338/MACC1/MET axis [9]. circ_000864 upregulates BTG2 to repress pancreatic cancer cell migration and invasion via interactions with miR-361-3p [10]. Additionally, hsa_circ_001653 is involved in pancreatic ductal adenocarcinoma progression through sponging miRNA-377 to upregulate HOXC6 [11]. Some circRNAs, such as circLDLRAD3, circ_001569 and hsa_circ_0013587, have also been used as biomarkers for pancreatic cancer diagnosis, prognosis, and molecular therapy [12–16]. These findings suggest that circRNAs play important roles in regulating pancreatic cancer. Therefore, further elucidation of the circRNA mechanism of pancreatic cancer is highly important for the diagnosis, treatment and prognosis of this disease.

N6-methyladenosine (m6A) methylation, the most prevalent form of epigenetic modification in RNA, is intricately linked to cell proliferation, metastasis and metabolism in various cancers, including pancreatic cancer [17, 18]. m6A methylation plays a crucial role in RNA posttranscriptional regulation, especially in inducing changes in the structural stability and expression level of RNA. Moreover, the stability and expression of circRNAs are also regulated by m6A methylation in different cancers [19, 20]. m6A methylation-modified circRNA-SORE sustains sorafenib resistance in hepatocellular carcinoma by regulating β-catenin signaling [21]. m6A methylation of circNSUN2 stabilizes HMGA2 to promote colorectal liver metastasis [22]. However, the relationship between circRNAs and m6A methylation in pancreatic cancer remains largely unclear.

The dyskeratosis congenita 1 (DKC1) gene was first identified because its mutation results in congenital dyskeratosis (DC), a rare inherited syndrome characterized by oral leukodystrophy, nail dystrophy, and unnatural reticular skin pigmentation [23]. Recent reports have suggested that DKC1 expression is dysregulated in diverse human cancers, affecting tumor growth or metastasis [24]. For example, DKC1 enhances angiogenesis and facilitates metastasis in colorectal cancer [25]. DKC1 aggravates gastric cancer cell migration and invasion [26]. More importantly, SENP3 has been reported to halt pancreatic ductal adenocarcinoma metastasis via deSUMOylation of DKC1 [27]. However, the relationship between circRNAs and DKC1 in pancreatic cancer remains unclear.

As reported previously, circCEACAM5 is highly expressed in gastric cancer tissues [28]. More importantly, Ye et al. identified 8807 m6A-circRNAs by analyzing m6A-seq data from 77 tissue samples from 58 individuals [29]. Among them, the expression of circCEACAM5 increased most significantly in pancreatic cancer tissues. In addition, METTL3 silencing led to a significant decrease in the relative abundance of circCEACAM5, suggesting that circCEACAM5 may contribute to pancreatic cancer progression through METTL3-mediated m6A methylation. Thus, our research aimed to clarify the function and mechanism of circCEACAM5 in pancreatic cancer and provide compelling evidence for the role of m6A methylation-mediated circRNAs in the treatment of this disease.

Methods and materials

Patient samples

We acquired paired samples of pancreatic cancer tumors and adjacent tissues from 32 patients between October 2019 and February 2022. The inclusion criteria were as follows: patients who were diagnosed with pancreatic cancer on the basis of pathology, cytology, and imaging and patients who had not received relevant antitumor treatment. Tumor classification followed the most recent American Joint Committee on Cancer TNM system. Upon collection, the samples were flash-frozen in liquid nitrogen and stored at − 80 °C. This research was conducted with the approval of Changshu Institute of Technology Ethics Committee, with all participants providing informed consent in line with the principles of the Helsinki Declaration.

Cellular models and experimental conditions

Our study utilized four human pancreatic cancer cell lines (BxPC-3, MIA-PaCa-2, AsPC-1, and PANC-1) and human pancreatic ductal epithelial (HPDE) cells, all of which were derived from Procell (Wuhan, China). The cancer cell lines were maintained in high-glucose DMEM (Gibco, USA, 11995065) enriched with 10% FBS (Biological Industries, 04-001-1A). HPDE cells were grown in RPMI 1640 medium (Gibco, USA, 11875093) supplemented similarly. All the cultures were maintained at 37 °C in a 5% CO_2 humidified environment.

For genetic manipulation experiments, AsPC-1 cells were transfected with various plasmids (500 ng per well in 6-well plates) via Lipofectamine 3000 (Thermo Fisher, L3000015) according to the manufacturer's protocol. These plasmids included overcircCEACAM5, shcircCEACAM5, overMETTL3, shMETTL3, overDKC1, and shDKC1. Subsequent analyses were performed 48 h posttransfection. The shRNA target sequence was as follows: sh-DKC1: 5′-CCG GCUGCACAAUGCUAUU-3′. sh-METTL3: 5′-GCAAGT ATGTTCACTATGAAA-3′.

Nucleic acid extraction and processing

We extracted total RNA from tissue and cell samples via TRIzol reagent (Thermo Fisher, 15596026). For the subcellular localization studies, the nuclear and cytoplasmic fractions were separated via a PARIS kit (Thermo Fisher, AM1921). Genomic DNA was isolated via a Genomic DNA Isolation Kit (TIANGEN Biotech, DP304-03).

To assess RNA stability, we subjected total RNA to treatment with either RNase R (3 U/μg, Abcam, ab286167) or actinomycin D (1 μg/mL, Sigma-Aldrich, A9415) at 37 °C for 10 min. After treatment, RNA was purified via an RNeasy MinElute Cleanup Kit (Qiagen, 74204) before RT−PCR analysis.

For PCR-based experiments, we amplified cDNA or gDNA via primers designed specifically for circCEACAM5. The resulting PCR products were visualized on 2% agarose gels in TAE buffer, with a 1000 bp DNA ladder (TransGen, BM101-01) for size reference. We confirmed the identity of the positive PCR products through Sanger sequencing.

Quantitative gene expression analysis

For quantitative analysis of gene expression, we isolated total RNA via TRIzol (Invitrogen, 15596026). The RNA was then reverse transcribed to cDNA using PrimeScript RT Master Mix (Takara, RR036A). Quantitative PCR was performed on an ABI 7500 real-time PCR system (Applied Biosystems) using SYBR Premix Ex Taq (Takara, RR420A). We calculated relative mRNA expression levels via the $2^{-\Delta\Delta CT}$ method, with β-actin serving as our internal control for normalization. All sequences of primers used were as follows: circCEACAM5: forward: 5′-CTCAGCTGGGGC CACTG-3′, reverse: 5′-GTGTCCGGCCCATCAGTC-3′; METTL3: forward: 5′-AAGCTGCACTTCAGACGAAT-3′, reverse: 5′-GGAATCACCTCCGACACTC-3′; GAPDH: forward: 5′-CAGCCAGGAGAAATCAAACAG-3′; reverse: 5′-GACTGAGTACCTGAACCGGC-3′.

Protein analysis

We extracted total protein from the samples via RIPA buffer (Thermo Fisher, 89900) and quantified it via a Bradford protein assay (BCA) kit (Thermo Fisher, 23225). For each sample, 30 μg of protein was resolved on 12% SDS−PAGE gels and transferred to PVDF membranes (Millipore, IPVH00010).

The membranes were blocked with 5% skim milk in TBST for 1 h at ambient temperature. We then probed the membranes with primary antibodies targeting METTL3 (1:1000, Abcam, #ab195352), CDK1 (1:1000, Cell Signaling Technology, #9116), or GAPDH (1:5000, Proteintech, #60004-1-Ig) overnight at 4 °C. Following TBST washes, the membranes were incubated with HRP-linked secondary antibodies (1:5000, Jackson ImmunoResearch, #111-035-003) for 2 h at room temperature.

We visualized the protein bands via a chemiluminescence imaging system (Biocompare) with enhanced chemiluminescence (ECL) reagents (Novex, WP20005) and quantified the band intensities via ImageJ software.

Assessment of cell viability

To evaluate cell viability, we employed the CCK8 assay. The cells were seeded in 96-well plates at a density of 2×10^3 cells per well in 100 μL of culture medium. At 24, 48, and 72 h postseeding, we added 10 μL of CCK-8 reagent (Sigma−Aldrich, 96,992) to each well. After a 2-h incubation at 37 °C, we measured the absorbance at 450 nm via a microplate reader.

Cell proliferation analysis

We assessed cell proliferation via a 5-ethynyl-2′-deoxyuridine (EdU) incorporation assay. The cells were cultured in medium supplemented with 50 μM EdU (Thermo Fisher, C10337) for 2 h. We subsequently fixed the cells with 50 μL of 4% paraformaldehyde for 30 min, followed by neutralization with 50 μL of 2 mg/mL glycine solution. The cell membranes were permeabilized with 100 μL of 0.5% Triton X-100 for 10 min.

After being washed with PBS, the cells were incubated with 100 μL of 1 × Apollo dye solution at room temperature for 30 min. We then counterstained the nuclei with 100 μL of Hoechst 33342 (1:2000 dilution) for 30 min. Images were acquired via a Nikon Eclipse Ti2 fluorescence microscope.

Apoptosis detection by flow cytometry

We assessed cellular apoptosis via flow cytometry. The cells were detached with 0.25% EDTA-free trypsin and suspended in binding buffer. The cell suspension was then treated with Annexin V-FITC and propidium iodide (PI) from an apoptosis detection kit (Life Technologies, V13242), with 5 μL of each stain added per 100 μL of cell suspension. After a 15-min incubation at room temperature in the dark, we analyzed the apoptotic rate via a BD FACSCanto II flow cytometer (BD Biosciences).

TUNEL assay

To further evaluate apoptosis, we employed the TdT-mediated dUTP nick end labeling (TUNEL) method with a commercial kit (Beyotime, C1086). The cells were grown to 75% confluence, fixed with 4% paraformaldehyde and permeabilized with a solution of 0.1% sodium citrate containing

0.1% Triton X-100. We then applied the TUNEL kit reagents to assess DNA fragmentation. Nuclear counterstaining was performed with DAPI (1:5000, Sigma-Aldrich, #D9542). We captured fluorescence images via a Nikon Eclipse Ti2 fluorescence microscope.

Cell invasion and migration assays

We evaluated cell invasion and migration capabilities via Transwell assays. For both assays, the cells were harvested and resuspended in serum-free DMEM. We seeded 2×10^4 cells in 200 μL of this medium into the upper chamber of Transwell inserts (8 μm pore size; Corning, 354480). The lower chamber contained 500 μL of medium supplemented with 20% FBS as a chemoattractant.

For invasion assays, the upper chamber was precoated with Matrigel. After a 24-h incubation at 37 °C, we carefully removed noninvaded cells from the upper surface of the membrane. The cells that had invaded through the membrane were fixed with 4% paraformaldehyde and visualized by staining with 0.1% crystal violet. We captured images via a light microscope.

RNA−protein interaction analysis

To investigate RNA−protein interactions, we employed a Magnetic RNA−Protein Pull-Down Kit (Thermo Fisher, 20164). We synthesized circCEACAM5 and its antisense RNA in vitro via T7 RNA polymerase and purified the transcripts with an RNeasy Mini Kit (Qiagen, 74104). The biotinylated RNA was then incubated with the cell lysates and streptavidin-coated magnetic beads for 1 h at 4 °C. After thorough washing, we eluted the bound proteins and analyzed them via western blotting.

Protein−RNA complex immunoprecipitation

We performed RNA immunoprecipitation (RIP) using a Magna RIP RNA-Binding Protein Immunoprecipitation Kit (Millipore, 17–700). The cell lysates were incubated for 6 h at 4 °C with magnetic beads conjugated to either anti-METTL3 antibody (Abcam, ab195352) or control IgG. Following incubation, we washed the beads and treated them with proteinase K. We then extracted the RNA via TRIzol reagent and quantified the circRNA abundance via RT−qPCR.

Subcellular RNA localization

To visualize the subcellular localization of specific RNAs, we conducted fluorescence in situ hybridization (FISH) using a commercial kit (RiboBio, Guangzhou, China). We fixed the cells with 4% paraformaldehyde and permeabilized them with 0.5% Triton X-100. The slides were then treated with proteinase K (20 μg/mL) for 10 min at room temperature, followed by incubation in prehybridization buffer for 1 h at 37 °C.

We performed hybridization overnight at 37 °C using a biotin-labeled probe (0.1 μg). After sequential washes with $2 \times$ SSC and $1 \times$ SSC, we incubated the slides with FITC-conjugated streptavidin (1:400 dilution) for 1 h at room temperature. Nuclei were counterstained with DAPI (1:5000, Sigma-Aldrich, D9542). We captured images via a Nikon Eclipse Ti2 fluorescence microscope.

In vivo tumor model

We conducted xenograft studies using five- to six-week-old female BALB/c nude mice (Beijing Vital River Company, Beijing, China) maintained under specific pathogen-free (SPF) conditions. The mice were kept in an independent ventilation cage, the temperature was strictly controlled at 23 ± 2 °C, the humidity was 50–60%, the diet and drinking water were provided ad libitum, the light conditions were automatically controlled, and the day and night cycle was 12 h. Following one week of acclimatization, we subcutaneously injected 1×10^7 AsPC-1 cells suspended in 100 μL of normal saline into each mouse's right flank.

Once the tumors reached approximately 100 mm^3, we randomly assigned the mice to treatment groups ($n = 5$ per group). Each group received intratumoral injections of 1×10^9 plaque-forming units (PFUs) of lentivirus carrying overcircCEACAM5, sh-circCEACAM5, or the control vector (Shanghai Genechem Co., Ltd., Shanghai, China). We administered injections every 3 days for a total of 5 treatments.

We measured tumor dimensions every 3 days via calipers and calculated the tumor volume via the following formula: $V = (L \times W^2)/2$, where V is the volume, L is the length, and W is the width. At 28 days postcell injection, we euthanized the mice via CO_2 inhalation and harvested the subcutaneous tumors for further analysis. All animal procedures were approved by the Animal Ethics Committee of Changshu Institute of Technology.

Histological analysis

We fixed the tumor tissues in 4% paraformaldehyde, embedded them in paraffin, and prepared 4-μm sections. For hematoxylin−eosin (H&E) staining, we deparaffinized and rehydrated the sections and then stained them with hematoxylin (5 min) followed by eosin (2 min). After dehydration and clearing, we mounted the sections with coverslips and examined them under a light microscope to assess histoarchitectural changes.

Protein expression in tissue samples

We performed immunohistochemical (IHC) staining on 4-μm-thick tissue sections. After deparaffinization and rehydration, we conducted antigen retrieval via citrate buffer (pH 6.0) at 95 °C for 20 min. We then quenched endogenous peroxidase activity with 3% H_2O_2 for 10 min and blocked nonspecific binding with 5% normal goat serum for 1 h at room temperature.

The sections were incubated overnight at 4 °C with an anti-Ki67 antibody (1:200, Abcam, ab15580). Following PBS washes, we applied an HRP-conjugated secondary antibody (1:500, Jackson ImmunoResearch, 111-035-003) for 1 h at room temperature. We visualized the signals via DAB substrate (Vector Laboratories, #SK-4100) and counterstained the nuclei with hematoxylin. Finally, we dehydrated, cleared, and mounted the sections with coverslips.

Data analysis

We conducted the statistical analyses via SPSS 21.0 software (IBM Corp., USA). The data are expressed as the means ± standard deviations (SDs). For comparisons between two groups, we employed Student's *t* test. For multiple group comparisons, we used one-way analysis of variance (ANOVA) followed by Tukey's post hoc test. We considered $p < 0.05$ to indicate statistical significance. All experiments were performed in triplicate and repeated at least three times to ensure reproducibility.

Results

circCEACAM5 is upregulated in pancreatic cancer

To investigate the status of circCEACAM5 in pancreatic cancer, we performed RT−qPCR analysis on both pancreatic cancer tissues and cell lines. circCEACAM5 expression in pancreatic cancer tumor tissues was significantly higher than that in adjacent normal tissues (Fig. 1A). As expected, circCEACAM5 expression was markedly increased in pancreatic cancer cell lines (BxPC-3, MIA-PaCa-2, AsPC-1, and PANC-1) compared with the normal pancreatic ductal epithelial cell line HPDE-C7 (Fig. 1B). Among the pancreatic cancer cell lines, AsPC-1 cells presented the highest level of circCEACAM5 expression, so AsPC-1 cells were selected for follow-up experiments.

Furthermore, correlation analysis revealed that higher levels of circCEACAM5 were significantly associated with elevated carcinoembryonic antigen levels, advanced clinical staging, positive N classification, the presence of venous invasion, and lymphatic metastasis (Supplementary Table 1). Collectively, these findings suggest that circCEACAM5 overexpression may promote pancreatic cancer progression.

Characterization of circCEACAM5

According to the circBase database, circCEACAM5 is derived from the CEACAM5 gene located on chromosome 19 (Fig. 2A). We confirmed the presence and sequence of circCEACAM5 via the use of divergent primers for amplification, followed by Sanger sequencing (Fig. 2B). The

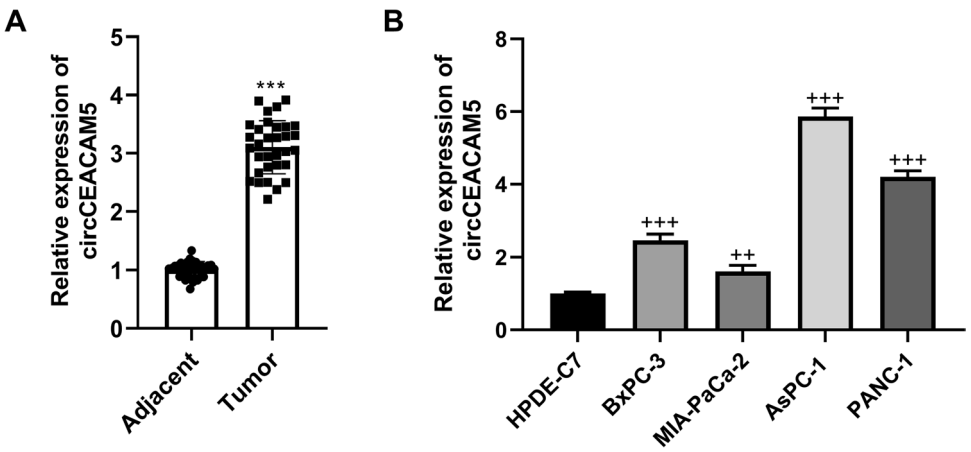

Fig. 1 Upregulation of circCEACAM5 in pancreatic cancer tissues and cell lines. **A** RT−qPCR analysis of circCEACAM5 expression in pancreatic cancer tissues and adjacent normal tissues ($n = 32$ per group). **B** RT−qPCR analysis of circCEACAM5 expression in pancreatic cancer cell lines and normal ductal epithelial cells (HPDE-C7). The data are presented as the means ± SDs from three independent experiments. $^{**}p < 0.01$, $^{***}p < 0.001$ compared with adjacent normal tissues or HPDE-C7 cells, respectively. Student's *t* test or one-way ANOVA was used for statistical analysis

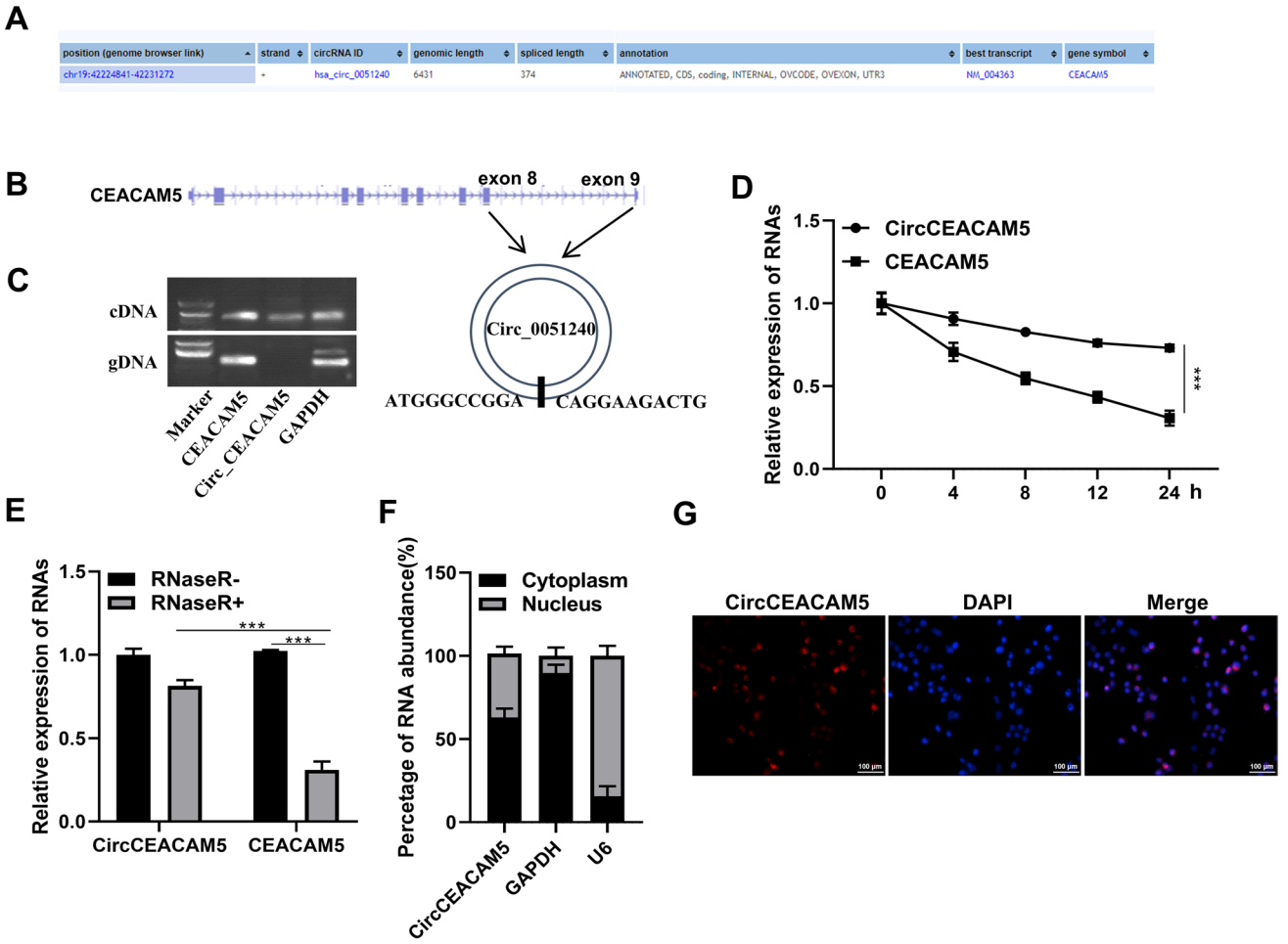

Fig. 2 Molecular characterization and subcellular localization of circCEACAM5. **A** Chromosomal location and best transcript of circCEACAM5 from the circBase database. **B** Sanger sequencing confirmation of circCEACAM5 amplification via divergent primers. **C** PCR analysis of circCEACAM5 in cDNA and gDNA via divergent primers. **D**, **E** Stability of circCEACAM5 and CEACAM5 mRNAs in AsPC-1 cells treated with Actinomycin D or RNase R. **F** RT−qPCR analysis of circCEACAM5 subcellular localization. **G** FISH detection of circCEACAM5 distribution in AsPC-1 cells. Scale bar = 100 μm. The data are presented as the means ± SDs from three independent experiments. ***$p < 0.001$. Student's *t* test or one-way ANOVA was used for statistical analysis

sequencing results were consistent with the circBase database annotation.

To validate the circular nature of circCEACAM5, we performed PCR on both cDNA and genomic DNA (gDNA) via divergent primers. Amplification products were observed only from cDNA templates, not from gDNA, supporting the circular structure of circCEACAM5 (Fig. 2C).

We then assessed the stability of circCEACAM5 compared with its linear counterpart, CEACAM5 mRNA. AsPC-1 cells were treated with actinomycin D to inhibit transcription. circCEACAM5 exhibited greater stability than did CEACAM5 mRNA (Fig. 2D). In addition, CEACAM5 mRNA was selectively degraded by RNase R, whereas circCEACAM5 was unaffected (Fig. 2E).

To determine the subcellular localization of circCEACAM5, we performed RT−qPCR analysis on subcellular fractions. CircCEACAM5 was distributed primarily in the cytoplasm rather than in the nucleus (Fig. 2F). This cytoplasmic localization was further confirmed by a fluorescence in situ hybridization (FISH) assay, which revealed that circCEACAM5 was present mainly in the cytoplasm of AsPC-1 cells, with a small fraction detected in the nucleus (Fig. 2G).

circCEACAM5 promotes AsPC-1 cell proliferation, invasion, and migration while inhibiting apoptosis

To determine the functional role of circCEACAM5 in pancreatic cancer, we conducted loss- and gain-of-function experiments in AsPC-1 cells. Cells were transfected with either circCEACAM5 overexpression plasmids or short hairpin RNA (shRNA) targeting circCEACAM5. RT−qPCR

analysis confirmed the successful overexpression or knockdown of circCEACAM5 in AsPC-1 cells (Fig. 3A).

Cell proliferation was assessed via the CCK-8 assay. Compared with the NC, circCEACAM5 overexpression significantly increased AsPC-1 cell proliferation, whereas circCEACAM5 knockdown reduced proliferation (Fig. 3B). Furthermore, EdU incorporation assays confirmed these findings, revealing a considerable increase in the number of EdU-positive cells upon circCEACAM5 overexpression and a decrease in the sh-circCEACAM5 group relative to the control group (Fig. 3C).

Transwell assays were utilized to evaluate cell migration and invasion capabilities. Both migratory and invasive abilities were significantly enhanced by circCEACAM5 overexpression, whereas they were suppressed by circCEACAM5 silencing compared with the respective controls (Fig. 3D, E).

To examine the effect of circCEACAM5 on apoptosis, we performed flow cytometry analysis. Elevated circCEACAM5 expression resulted in reduced apoptosis, whereas the sh-circCEACAM5 group exhibited increased apoptosis relative to the control group (Fig. 3F).

Collectively, these findings suggest that circCEACAM5 promotes malignant phenotypes in AsPC-1 cells, including enhanced proliferation, migration, and invasion, while suppressing apoptosis.

circCEACAM5 promotes pancreatic cancer tumor growth in vivo

To extend our in vitro findings and investigate the impact of circCEACAM5 on pancreatic cancer progression in a more physiologically relevant context, we established xenograft tumor mouse models. Consistent with the results of our cell culture experiments, RT−qPCR analysis confirmed the successful modulation of circCEACAM5 expression in tumor tissues following the injection of lentiviral vectors. Compared with those from the negative control (NC) group, tumors derived from cells overexpressing circCEACAM5 presented significantly elevated circCEACAM5 levels, whereas those from circCEACAM5-silenced cells presented reduced circCEACAM5 expression (Fig. 4A).

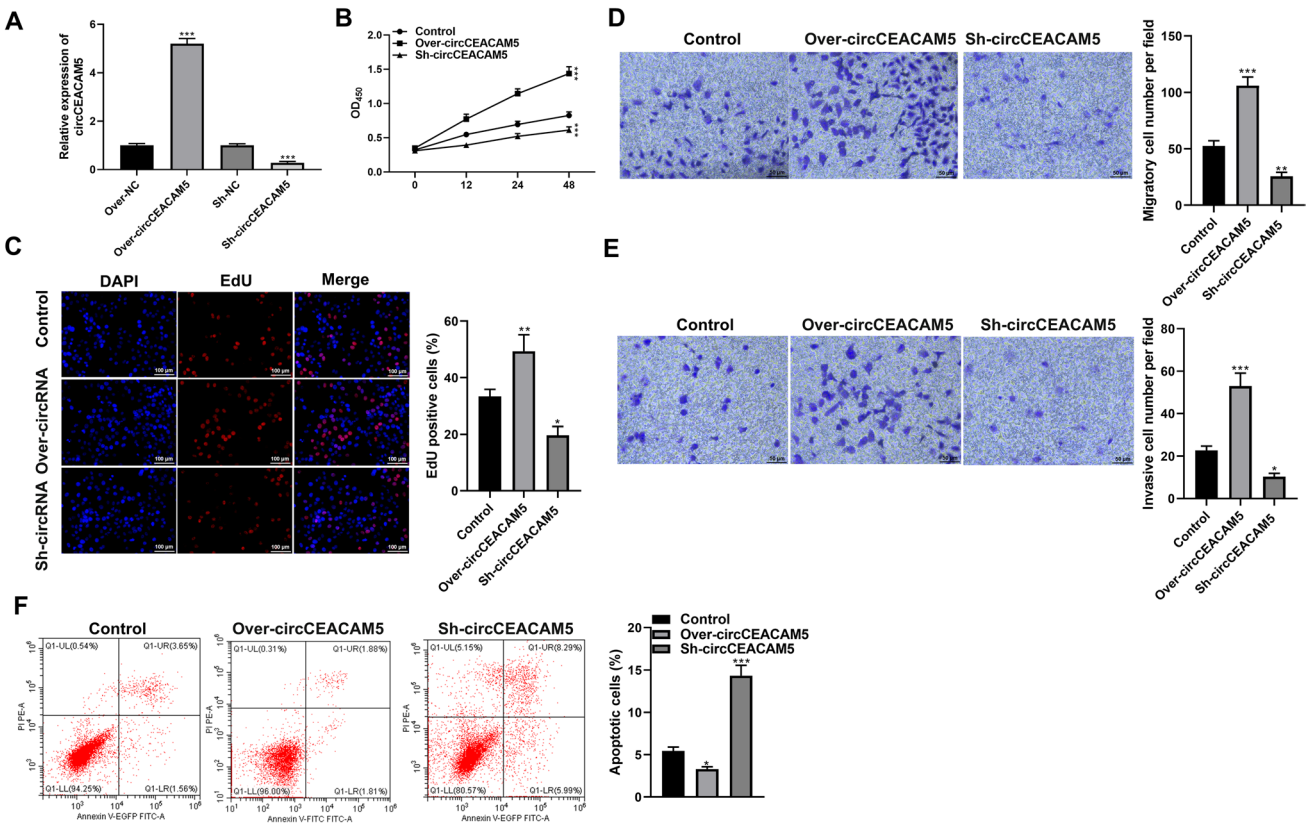

Fig. 3 circCEACAM5 enhances proliferation, invasion, and migration while suppressing apoptosis in pancreatic cancer cells. **A** RT−qPCR analysis of circCEACAM5 expression in AsPC-1 cells following circCEACAM5 overexpression or knockdown. **B** CCK-8 assay of AsPC-1 cell proliferation. **C** EdU incorporation assay. Scale bar = 100 μm. **D**, **E** Transwell migration and invasion assays. Scale bar = 50 μm. **F** Flow cytometry analysis of apoptosis. The data are presented as the means ± SDs from three independent experiments. $*p<0.05$, $**p<0.01$, $***p<0.001$ compared with the respective controls. One-way ANOVA was used for statistical analysis

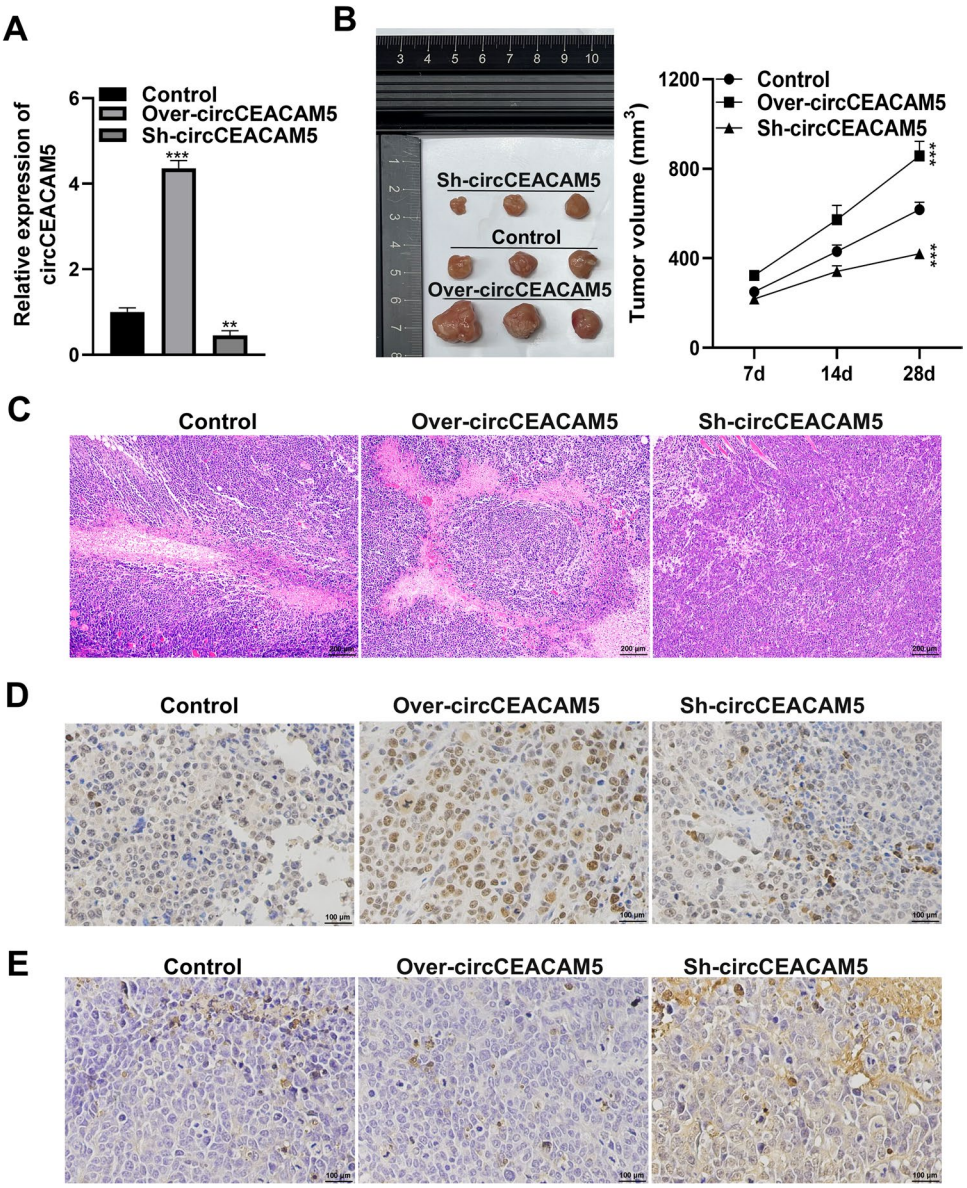

Fig. 4 circCEACAM5 promotes pancreatic tumor growth and inhibits apoptosis in vivo. **A** RT−qPCR analysis of circCEACAM5 expression in xenograft tumors. **B** Tumor volume measurements over time. **C** H&E staining of tumor sections. Scale bar = 100 µm. **D**, **E** Ki-67 and TUNEL staining of tumor sections. Scale bar = 100 µm. The data are presented as the means ± SDs ($n = 5$ mice per group). $^{**}p < 0.01$, $^{***}p < 0.001$ compared with the respective controls. One-way ANOVA was used for statistical analysis

The effects of circCEACAM5 modulation on tumor growth mirrored our in vitro proliferation results. Compared with NC, circCEACAM5 overexpression led to a marked increase in tumor size, whereas circCEACAM5 silencing significantly reduced tumor size (Fig. 4B). These findings underscore the oncogenic potential of circCEACAM5 in vivo.

Histopathological analysis via H&E staining revealed increased necrosis in tumor tissues overexpressing circCEACAM5, whereas tumors with circCEACAM5 knockdown presented reduced necrosis (Fig. 4C). These findings suggest that circCEACAM5 may influence tumor tissue architecture and promote tumor growth.

To further corroborate our in vitro proliferation data, we performed Ki-67 immunohistochemical staining. Consistent with our previous findings, circCEACAM5 overexpression promoted cell proliferation, as evidenced by increased Ki-67-positive cells, whereas circCEACAM5 suppression inhibited proliferation relative to that of the controls (Fig. 4D).

In line with our in vitro apoptosis results, the TUNEL assay revealed that apoptosis was inhibited in tumor tissues overexpressing circCEACAM5, whereas it was promoted in tissues with suppressed circCEACAM5 expression compared with controls (Fig. 4E).

Collectively, these in vivo results validate and extend our in vitro findings, demonstrating that circCEACAM5 promotes pancreatic cancer tumor growth by increasing proliferation and suppressing apoptosis in a physiologically relevant model system.

METTL3 mediates m6A RNA methylation of circCEACAM5

To understand the possible regulatory mechanism of circCEACAM5, we examined m6A RNA methylation mediated by METTL3. Bioinformatic analysis via the SRAMP algorithm revealed multiple putative m6A modification sites within the circCEACAM5 sequence (Fig. 5A).

METTL3 expression levels were quantified in both pancreatic cancer tissues and cell lines. RT−qPCR analysis revealed a significant increase in METTL3 mRNA levels in pancreatic cancer tissues compared with those in adjacent normal tissues (Fig. 5B). Similarly, Western blot analysis of pancreatic cancer cell lines (AsPC-1, PANC-1, and MIA PaCa-2) revealed elevated METTL3 protein levels relative to those in the normal pancreatic epithelial cell line HPDE6-C7 (Fig. 5C).

M6A-specific RNA immunoprecipitation (MeRIP) assays were performed to assess the m6A methylation status of circCEACAM5. In AsPC-1 cells, a significant increase in the m6A level of circCEACAM5 was observed compared with that in HPDE6-C7 cells (Fig. 5D). To confirm the role of METTL3 in this modification, siRNA-mediated METTL3 knockdown was performed on AsPC-1 cells. This resulted in a marked reduction in the m6A levels of circCEACAM5 relative to those in cells transfected with scrambled siRNA (Fig. 5E).

The direct interaction between METTL3 and circCEACAM5 was investigated via RNA pull-down assays coupled with Western blot analysis. Compared with the control probes, the biotinylated circCEACAM5 probes significantly enriched the METTL3 protein (Fig. 5F), indicating specific binding between METTL3 and circCEACAM5.

To further establish a regulatory link between METTL3 and circCEACAM5, we modulated METTL3 expression levels in AsPC-1 cells. Lentivirus-mediated overexpression of METTL3 led to a significant increase in circCEACAM5 levels, as measured by RT−qPCR. Conversely, METTL3 silencing via shRNA resulted in a substantial decrease in circCEACAM5 expression (Fig. 5G). These findings collectively suggest that METTL3 plays a direct regulatory role in regulating circCEACAM5 expression, likely through m6A modification.

METTL3 orchestrates key cellular processes in AsPC-1 cells

To explore the role of METTL3 in pancreatic cancer, we performed functional modulation experiments in AsPC-1 cells. Western blot analysis confirmed the effective alteration in METTL3 expression, revealing distinct protein level

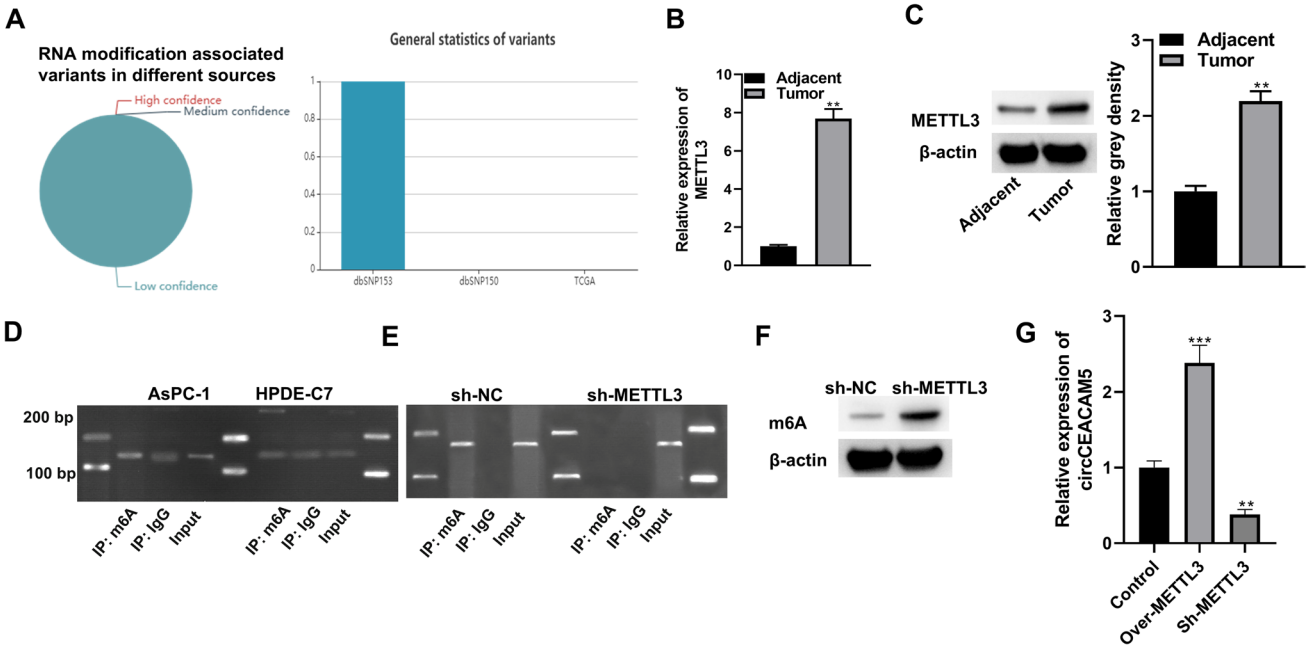

Fig. 5 METTL3-mediated m6A modification regulates circCEACAM5 expression in pancreatic cancer. **A** Predicted m6A modification sites in circCEACAM5. **B**, **C** RT−qPCR analysis of METTL3 expression in pancreatic cancer tissues and cell lines. **D** m6A-specific immunoprecipitation of circCEACAM5 in AsPC-1 cells. **E** m6A-specific immunoprecipitation of circCEACAM5 following METTL3 knockdown. **F** RNA pull-down assay showing that circCEACAM5 binds to METTL3. **G** RT−qPCR analysis of circCEACAM5 expression following METTL3 modulation. The data are presented as the means ± SDs from three independent experiments. $^{**}p < 0.01$, $^{***}p < 0.001$ compared with the respective controls. Student's t test or one-way ANOVA was used for statistical analysis

differences between the overexpression, knockdown, and control groups (Fig. 6A).

METTL3 overexpression significantly promoted AsPC-1 cell proliferation, while its knockdown led to a marked decrease in cell growth, as shown by CCK-8 assays (Fig. 6B). These findings were further supported by the results of the EdU assays, which revealed a significant increase in the number of EdU-positive cells with METTL3 upregulation and a corresponding decrease in the number of cells in the knockdown group compared with those in the control group (Fig. 6C).

Cell migration and invasion assays revealed that overexpression of METTL3 increased migration and invasion, whereas silencing METTL3 significantly impaired these functions (Fig. 6D).

Additionally, flow cytometry analysis demonstrated that METTL3 upregulation reduced apoptosis, whereas METTL3 downregulation significantly increased apoptotic cell death relative to that in the controls (Fig. 6E).

These results imply that METTL3 is a key regulator of AsPC-1 cell behaviors, including enhanced proliferation, migration, invasion, and resistance to apoptosis, contributing to the aggressive nature of pancreatic cancer.

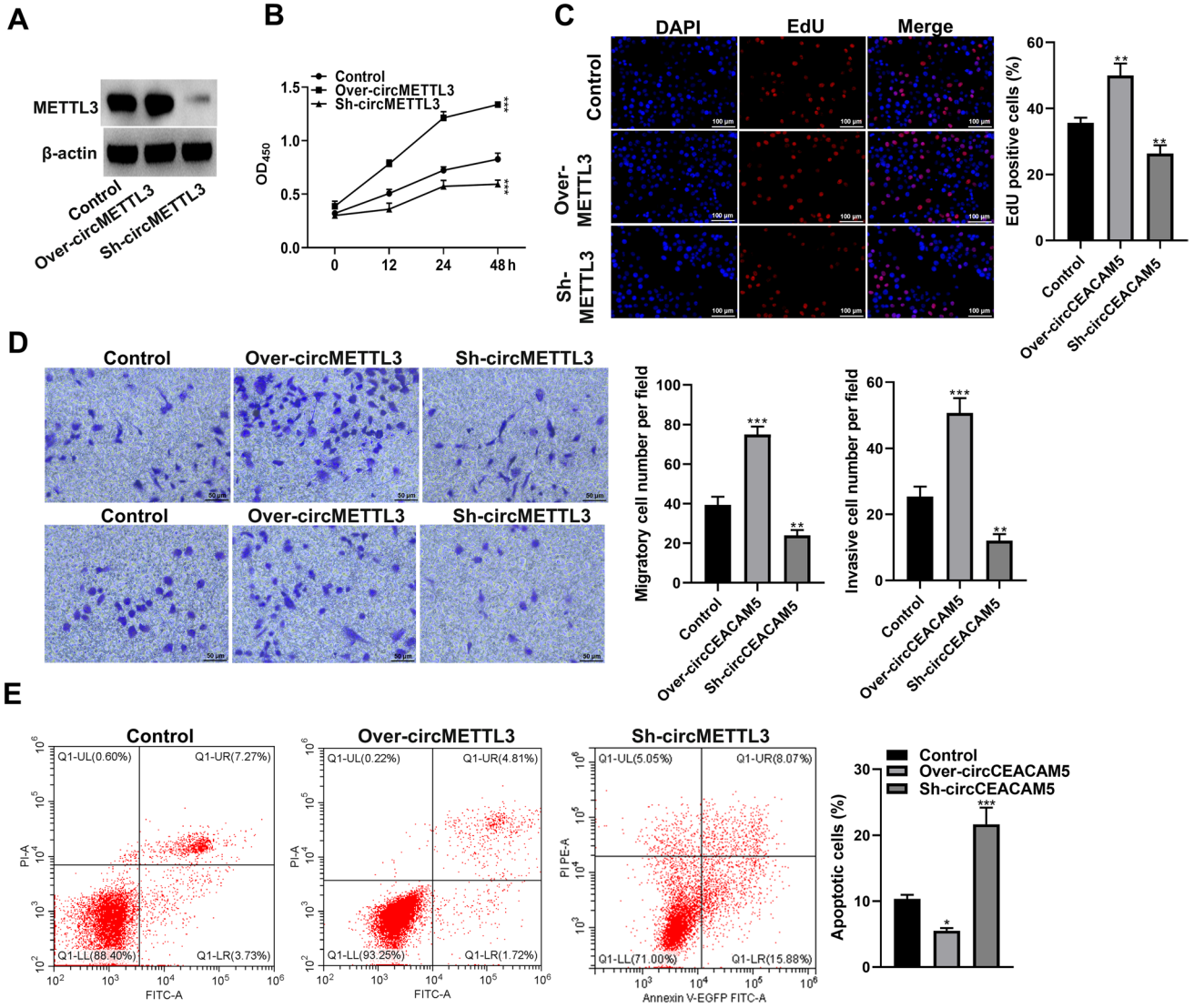

Fig. 6 METTL3 promotes aggressive phenotypes in pancreatic cancer cells. **A** Western blot analysis of METTL3 protein levels following overexpression or knockdown. **B** CCK-8 assay of AsPC-1 cell proliferation. **C** EdU incorporation assay. Scale bar = 100 μm. **D** Transwell migration and invasion assays. Scale bar = 50 μm. **E** Flow cytometry analysis of apoptosis. The data are presented as the means ± SDs from three independent experiments. $^{**}p < 0.01$, $^{***}p < 0.001$ compared with the respective controls. One-way ANOVA was used for statistical analysis

circCEACAM5 exhibits specific interactions with DKC1 in AsPC-1 cells

To elucidate the molecular mechanism underlying circCEACAM5 function, we employed bioinformatic approaches to identify potential RNA binding proteins (RBPs) associated with this circular RNA. Analysis via the Starbase2 database highlighted two candidate RBPs: DKC1 and UPF1 (Fig. 7A).

To experimentally validate these predicted interactions, we conducted RNA pull-down assays using biotinylated circCEACAM5 and its antisense RNA as a control. Western blot analysis of the pulled-down fractions revealed a robust and specific association between DKC1 and circCEACAM5, whereas no detectable binding was detected with the antisense RNA control (Fig. 7B). Intriguingly, UPF1 failed to demonstrate binding affinity for either circCEACAM5 or antisense RNA (Fig. 7C), suggesting that the computationally predicted interaction with UPF1 may not be physiologically relevant in our experimental system.

To further corroborate the circCEACAM5-DKC1 interaction, we performed RNA immunoprecipitation (RIP) assays. Quantitative PCR analysis of the immunoprecipitated samples revealed significant enrichment of circCEACAM5 in the DKC1-bound fraction compared with the IgG control (Fig. 7D). This finding provides additional evidence for the specificity and robustness of the circCEACAM5-DKC1 interaction in AsPC-1 cells.

To explore the potential regulatory relationship between circCEACAM5 and DKC1, we examined the impact of circCEACAM5 depletion on DKC1 expression. siRNA-mediated knockdown of circCEACAM5 in AsPC-1 cells resulted in a substantial reduction in DKC1 protein levels relative to those in cells transfected with nontargeting control siRNA (Fig. 7E). These findings suggest that circCEACAM5 may play a role in modulating DKC1 expression or stability.

A

RBP	GeneID	GeneName	GeneType	ClusterNum	ClipExpNum	ClipSiteNum
DKC1	NM_004363	CEACAM5	circRNA	1	1	1
UPF1	NM_004363	CEACAM5	circRNA	1	1	1

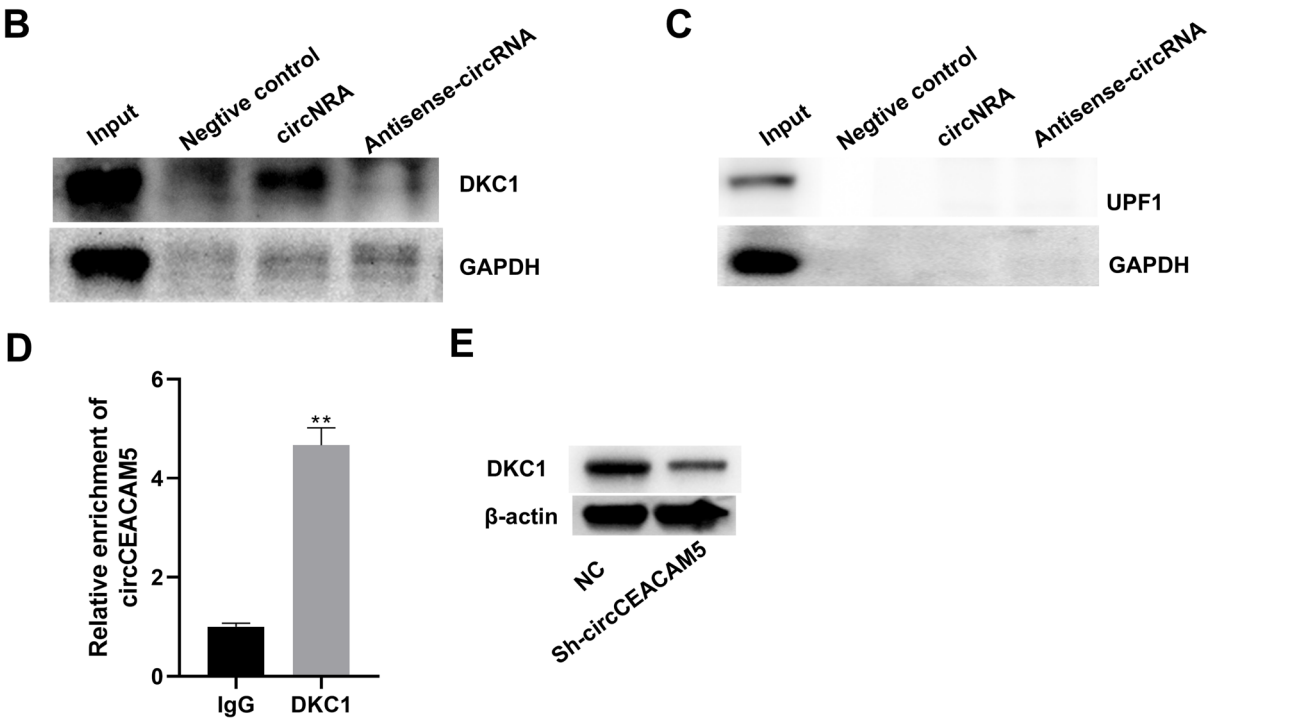

Fig. 7 circCEACAM5 specifically interacts with DKC1 in pancreatic cancer cells. **A** Predicted RNA-binding proteins (RBPs) for circCEACAM5 via starBase2. **B**, **C** RNA pull-down assays showing the associations of DKC1 and UPF1 with circCEACAM5. **D** RIP assay detecting circCEACAM5 enrichment via anti-DKC1 or IgG antibodies. **E** Western blot analysis of DKC1 protein levels following circCEACAM5 knockdown. The data are presented as the means ± SDs from three independent experiments. $^{**}p < 0.01$ compared with the IgG control. Student's t test was used for statistical analysis

Collectively, these findings establish a specific and functional interaction between circCEACAM5 and DKC1 in AsPC-1 cells.

DKC1 influences AsPC-1 cell behavior via the circCEACAM5 interaction

To elucidate the functional role of DKC1 in pancreatic cancer and its relationship with circCEACAM5, we performed a series of experiments in AsPC-1 cells. Western blot analysis confirmed the successful modulation of DKC1 protein levels under DKC1 overexpression and knockdown conditions (Fig. 8A).

CCK-8 assays revealed that DKC1 overexpression significantly enhanced AsPC-1 cell proliferation, whereas DKC1 knockdown reduced proliferation compared with that in the control groups. Concurrent manipulation of circCEACAM5 levels attenuated these proliferative effects (Fig. 8B).

Transwell assays demonstrated that both migratory and invasive abilities were significantly promoted by DKC1 overexpression and inhibited by DKC1 suppression relative to those of the controls. Alterations in circCEACAM5 expression mitigated these changes in cell motility and invasion (Fig. 8C, D).

Flow cytometry analysis revealed that DKC1 overexpression resulted in reduced apoptosis, whereas DKC1 silencing increased apoptosis compared with that of the controls. Modulation of circCEACAM5 levels counteracted the observed effects on apoptosis (Fig. 8E).

These findings demonstrate that DKC1 promotes proliferation, migration, and invasion while suppressing apoptosis in AsPC-1 cells. The dependence of these effects on circCEACAM5 suggests a functional interplay between DKC1 and circCEACAM5 in regulating pancreatic cancer cell behavior.

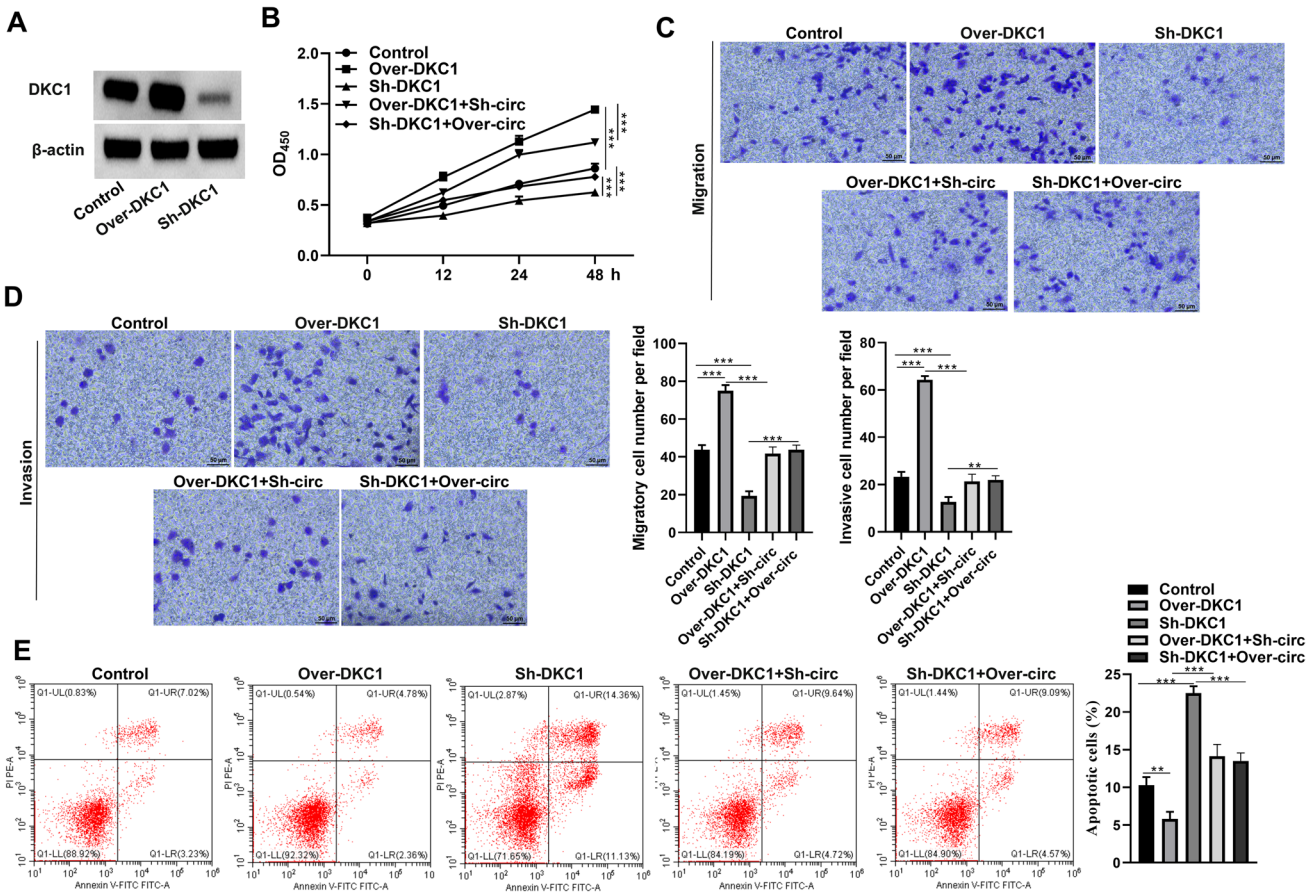

Fig. 8 DKC1 mediates the oncogenic effects of circCEACAM5 in pancreatic cancer cells. **A** Western blot analysis of DKC1 protein levels following DKC1 overexpression. **B** CCK-8 assay of AsPC-1 cell proliferation. **C**, **D** Transwell migration and invasion assays. Scale bar = 50 μm. **E** Flow cytometry analysis of apoptosis. The data are presented as the means ± SDs from three independent experiments. $^{**}p < 0.01$, $^{***}p < 0.001$ compared with the indicated groups. One-way ANOVA was used for statistical analysis

Discussion

Pancreatic cancer, a severe digestive tract malignancy, is associated with no obvious clinical symptoms in its early stages and is prone to metastasis. Consequently, most patients are diagnosed with stage III or IV disease [30, 31]. Recent studies have shown that pancreatic cancer is a complex disease regulated by multiple genes, signaling pathways, and growth factors [32]. Thus, only in-depth investigations into the mechanisms underlying pancreatic cancer progression can provide new directions for targeted therapies. In this study, circCEACAM5 was upregulated in tumor tissue and cells. High circCEACAM5 levels in pancreatic cancer were associated with poor clinicopathological manifestations. Mechanistically, METTL3-mediated m6A methylation of circCEACAM5 promoted pancreatic cancer progression by increasing DKC1 expression.

The high stability, cross-species conservation, and tissue specificity of circular RNAs (circRNAs) have positioned them as promising molecular biomarkers and therapeutic targets. CircRNAs play vital roles in pancreatic cancer progression [33]. For instance, circRHOT1 is upregulated in pancreatic cancer and promotes cell proliferation and invasion [34]. Huang et al. reported that exosomal circ-IARS from pancreatic cancer cells enhances tumor metastasis by regulating endothelial monolayer permeability [35]. Similarly, circFOXK2/miR-942 modulates pancreatic ductal adenocarcinoma growth and metastasis by interacting with RNA-binding proteins [36]. Consistent with these findings, we observed elevated circCEACAM5 levels in pancreatic cancer tissues and cells, with high expression linked to unfavorable clinicopathological features. Further analysis revealed that circCEACAM5 overexpression enhanced AsPC-1 cell proliferation, invasion, and migration; suppressed apoptosis; and promoted tumor growth in pancreatic cancer models.

m6A methylation influences pancreatic cancer progression by modulating cancer-related biological functions [37]. For example, Liu et al. demonstrated that m6A methylation regulates hypoxia-induced glycolytic metabolism in pancreatic cancer [38]. Tang et al. reported that m6A-related genes are critical for the prognosis and immune microenvironment of pancreatic adenocarcinoma [39]. Moreover, m6A modification regulates circRNA expression by affecting precursor cleavage, nuclear export, translation, and stability [40]. For example, Liu et al. reported that m6A modification-regulated circ-CCT3 promoted hepatocellular carcinoma progression [41]. Li et al. demonstrated that m6A modification-modified circTEAD1 promoted chordoma tumorigenesis [42]. Wang et al. reported that ALKBH5-mediated m6A modification of circFOXP1 promoted gastric cancer progression [43]. Our analysis revealed that circCEACAM5 was downregulated when METTL3 was silenced, suggesting that circCEACAM5 could be regulated by METTL3. Our study revealed that METTL3 directly participates in the m6A methylation of circCEACAM5. Consistent with our findings, METTL3-mediated m6A modification of circGLIS3 promotes prostate cancer progression [44], and METTL3-dependent m6A methylation of circ_0008345 contributes to the progression of colorectal cancer [45]. Indeed, METTL3 functions as an oncogene underlying pancreatic cancer progression and facilitates pancreatic cancer cell chemoradioresistance, proliferation, and invasion [46]. Supporting these observations, we demonstrated that overexpression of METTL3 facilitated AsPC-1 cell proliferation, invasion and migration while repressing cell apoptosis.

Additionally, circRNAs regulate disease progression by interacting with key proteins, such as RNA-binding proteins (RBPs), to modulate gene expression [47]. Here, we identified DKC1 as an RBP partner of circCEACAM5. DKC1 acts as an oncogene in various cancers. For instance, Hou et al. showed that DKC1 promotes HIF-1α transcription, enhancing angiogenesis and metastasis in colorectal cancer [25]. Similarly, DKC1 overexpression drives proliferation, migration, and invasion via the NF-κB pathway in clear cell renal cell carcinoma, suggesting its potential as a therapeutic target [48]. Khloud et al. linked DKC1 to high tumor grade, high nucleolar score, and poor prognosis in patients with breast cancer [49]. However, its role in pancreatic cancer remains unclear. Our findings demonstrate that DKC1 overexpression counteracts the effects of circCEACAM5 silencing on AsPC-1 cell proliferation, invasion, migration, and apoptosis. Comparable mechanisms have been reported elsewhere, such as circARID1A binding to IGF2BP3 in gastric cancer [50] and circACTN4 recruiting YBX1 in intrahepatic cholangiocarcinoma [51].

In conclusion, we demonstrated that increased expression of circCEACAM5 is linked to unfavorable clinicopathological characteristics in patients with pancreatic cancer. Our mechanistic studies revealed that METTL3-mediated m6A methylation of circCEACAM5 promoted pancreatic cancer progression via upregulation of DKC1 expression. These findings indicate that targeting circCEACAM5 and METTL3 could serve as biomarkers or therapeutic targets for pancreatic cancer. Moreover, METTL3 inhibitors or circCEACAM5 knockdown approaches may complement existing therapies for pancreatic cancer. Future studies should focus on validating these findings in larger patient cohorts and exploring the potential of circCEACAM5-targeted therapies in clinical settings.

Supplementary Information The online version contains supplementary material available at https://doi.org/10.1007/s00018-025-05653-5.

Acknowledgements Not applicable.

Author contributions Jie Zhang: Conceptualization, Data curation, Formal analysis, Investigation, Methodology, Software, Validation, Visualization, Writing—original draft preparation, Writing—review & editing. Wenxue Sun: Conceptualization, Data curation, Formal analysis, Investigation, Methodology, Software, Validation, Visualization, Writing—review & editing. Wenda Wu: Conceptualization, Data curation, Formal analysis, Software, Validation, Visualization, Writing—review & editing. Zihui Qin: Conceptualization, Data curation, Formal analysis, Software, Validation, Visualization, Writing—review & editing. Ben Wei: Conceptualization, Data curation, Formal analysis, Software, Validation, Visualization, Writing—review & editing. Tushuai Li: Conceptualization, Funding acquisition, Project administration, Resources, Supervision, Writing—original draft preparation, Writing—review & editing.

Funding This research was supported by the General Program of China Postdoctoral Science Foundation (2022M711369), the China-CEEC Joint University Education Project (202010), the National Natural Science Foundation of China (32172922, 31972741), the Natural Science Foundation of Jiangsu Province of China (BK20211216), the Suzhou Science and Technology Council (SNG201907) and the Universities Natural Science Foundation of Jiangsu Province (20KJB330002).

Availability of data and materials The data presented in this study are available upon request from the corresponding author.

Declarations

Conflict of interests The authors declare that they have no conflicts of interest.

Ethics approval and consent to participate This study was conducted in accordance with the Declaration of Helsinki and approved by the Ethics Committee of Changshu Institute of Technology. Informed consent was obtained from all the subjects involved in the study. All animal experiments were performed in compliance with the Changshu Institute of Technology guidelines for the care and use of animals and were approved by the Institutional Animal Care and Use Committee of Changshu Institute of Technology.

Consent for publication Not applicable.

References

1. Rawla P, Sunkara T, Gaduputi V (2019) Epidemiology of pancreatic cancer: global trends, etiology and risk factors. World J Oncol 10(1):10–27
2. Roth MT, Cardin DB, Berlin JD (2020) Recent advances in the treatment of pancreatic cancer. F1000 Res 9:131
3. Neoptolemos JP et al (2018) Therapeutic developments in pancreatic cancer: current and future perspectives. Nat Rev Gastroenterol Hepatol 15(6):333–348
4. Zhao Z, Liu W (2020) Pancreatic cancer: a review of risk factors, diagnosis, and treatment. Technol Cancer Res Treat 19:1533033820962117
5. Kristensen LS et al (2022) The emerging roles of circRNAs in cancer and oncology. Nat Rev Clin Oncol 19(3):188–206
6. Kristensen LS et al (2019) The biogenesis, biology and characterization of circular RNAs. Nat Rev Genet 20(11):675–691
7. Jin X et al (2019) Baicalin mitigates cognitive impairment and protects neurons from microglia-mediated neuroinflammation via suppressing NLRP3 inflammasomes and TLR4/NF-κB signaling pathway. CNS Neurosci Ther 25(5):575–590
8. Li J et al (2015) Circular RNAs in cancer: novel insights into origins, properties, functions and implications. Am J Cancer Res 5(2):472–480
9. Li Z et al (2018) Tumor-released exosomal circular RNA PDE8A promotes invasive growth via the miR-338/MACC1/MET pathway in pancreatic cancer. Cancer Lett 432:237–250
10. Huang L et al (2020) CircRNA_000864 upregulates B-cell translocation gene 2 expression and represses migration and invasion in pancreatic cancer cells by binding to miR-361-3p. Front Oncol 10:547942
11. Shi H et al (2020) Retracted: hsa_circ_001653 implicates in the development of pancreatic ductal adenocarcinoma by regulating MicroRNA-377-mediated HOXC6 axis. Mol Ther Nucleic Acids 20:252–264
12. Zhang H-D et al (2017) CircRNA: a novel type of biomarker for cancer. Breast Cancer 25(1):1–7
13. Rong Z et al (2021) Circular RNA in pancreatic cancer: a novel avenue for the roles of diagnosis and treatment. Theranostics 11(6):2755–2769
14. Yang F et al (2017) Circular RNA circ-LDLRAD3 as a biomarker in diagnosis of pancreatic cancer. World J Gastroenterol 23(47):8345–8354
15. Shen X et al (2021) Identification of Circ_001569 as a potential biomarker in the diagnosis and prognosis of pancreatic cancer. Technol Cancer Res Treat 20:1533033820983302
16. Xu K et al (2021) Increased levels of circulating circular RNA (Hsa_Circ_0013587) may serve as a novel biomarker for pancreatic cancer. Biomark Med 15(12):977–985
17. Di Timoteo G et al (2020) Modulation of circRNA metabolism by m6A modification. Cell Rep 31(6):107641
18. Chen S et al (2021) CLK1/SRSF5 pathway induces aberrant exon skipping of METTL14 and cyclin L2 and promotes growth and metastasis of pancreatic cancer. J Hematol Oncol 14(1):60
19. Zhang L et al (2020) The role of N6-methyladenosine (m6A) modification in the regulation of circRNAs. Mol Cancer 19(1):105
20. Zhang C et al (2020) Circular RNA expression profile and m6A modification analysis in poorly differentiated adenocarcinoma of the stomach. Epigenomics 12(12):1027–1040
21. Xu J et al (2020) N6-methyladenosine-modified CircRNA-SORE sustains sorafenib resistance in hepatocellular carcinoma by regulating β-catenin signaling. Mol Cancer 19(1):163
22. Chen R-X et al (2019) N6-methyladenosine modification of circNSUN2 facilitates cytoplasmic export and stabilizes HMGA2 to promote colorectal liver metastasis. Nat Commun 10(1):4695

23. Kan G et al (2021) Dual Inhibition of DKC1 and MEK1/2 synergistically restrains the growth of colorectal cancer cells. Adv Sci (Weinh) 8(10):2004344
24. Liu XY, Tan Q, Li LX (2023) A pan-cancer analysis of Dyskeratosis congenita 1 (DKC1) as a prognostic biomarker. Hereditas 160(1):38
25. Hou P et al (2020) DKC1 enhances angiogenesis by promoting HIF-1α transcription and facilitates metastasis in colorectal cancer. Br J Cancer 122(5):668–679
26. Chen H et al (2024) DKC1 aggravates gastric cancer cell migration and invasion through up-regulating the expression of TNFAIP6. Funct Integr Genomics 24(2):38
27. Wu X et al (2023) SUMO specific peptidase 3 halts pancreatic ductal adenocarcinoma metastasis via deSUMOylating DKC1. Cell Death Differ 30(7):1742–1756
28. Hossain MT et al (2022) Identification of circRNA biomarker for gastric cancer through integrated analysis. Front Mol Biosci 9:857320
29. Ye Y et al (2021) Genome-wide identification and characterization of circular RNA m6A modification in pancreatic cancer. Genome Med 13(1):183
30. Zhang L, Sanagapalli S, Stoita A (2018) Challenges in diagnosis of pancreatic cancer. World J Gastroenterol 24(19):2047–2060
31. McGuigan A et al (2018) Pancreatic cancer: a review of clinical diagnosis, epidemiology, treatment and outcomes. World J Gastroenterol 24(43):4846–4861
32. Loveday BPT, Lipton L, Thomson BNJ (2019) Pancreatic cancer: an update on diagnosis and management. Austr J Gen Pract 48(12):826–831
33. Zhang Q et al (2019) Circular RNA expression in pancreatic ductal adenocarcinoma. Oncol Lett 18(3):2923–2930
34. Qu S et al (2018) Circular RNA circRHOT1 is upregulated and promotes cell proliferation and invasion in pancreatic cancer. Epigenomics 11(1):53–63
35. Li J et al (2018) Circular RNA IARS (circ-IARS) secreted by pancreatic cancer cells and located within exosomes regulates endothelial monolayer permeability to promote tumor metastasis. J Exp Clin Cancer Res 37(1):177
36. Wong CH et al (2020) CircFOXK2 promotes growth and metastasis of pancreatic ductal adenocarcinoma by complexing with RNA-binding proteins and sponging MiR-942. Can Res 80(11):2138–2149
37. Hou J et al (2020) Gene signature and identification of clinical trait-related m6 A regulators in pancreatic cancer. Front Genet 11:522
38. Liu X et al (2023) m6A methylation regulates hypoxia-induced pancreatic cancer glycolytic metabolism through ALKBH5-HDAC4-HIF1α positive feedback loop. Oncogene 42(25):2047–2060
39. Tang R et al (2020) The role of m6A-related genes in the prognosis and immune microenvironment of pancreatic adenocarcinoma. PeerJ 8:e9602
40. Xu D et al (2024) N(6)-methyladenosine modification of circular RNA circASH2L suppresses growth and metastasis in hepatocellular carcinoma through regulating hsa-miR-525-3p/MTUS2 axis. J Transl Med 22(1):1026
41. Liu H et al (2023) m(6)A-modification regulated circ-CCT3 acts as the sponge of miR-378a-3p to promote hepatocellular carcinoma progression. Epigenetics 18(1):2204772
42. Li H et al (2024) N6-methyladenosine-modified circTEAD1 stabilizes Yap1 mRNA to promote chordoma tumorigenesis. Clin Transl Med 14(4):e1658
43. Wang S et al (2024) ALKBH5-mediated m6A modification of circFOXP1 promotes gastric cancer progression by regulating SOX4 expression and sponging miR-338-3p. Commun Biol 7(1):565
44. Cheng X et al (2024) METTL3-mediated m(6)A modification of circGLIS3 promotes prostate cancer progression and represents a potential target for ARSI therapy. Cell Mol Biol Lett 29(1):109
45. Hou C et al (2024) METTL3-induced circ_0008345 contributes to the progression of colorectal cancer via the microRNA-182-5p/CYP1A2 pathway. BMC Cancer 24(1):728
46. Taketo K et al (2017) The epitranscriptome m6A writer METTL3 promotes chemo- and radioresistance in pancreatic cancer cells. Int J Oncol 52(2):621–629
47. Conn SJ et al (2015) The RNA binding protein quaking regulates formation of circRNAs. Cell 160(6):1125–1134
48. Zhang M et al (2018) DKC1 serves as a potential prognostic biomarker for human clear cell renal cell carcinoma and promotes its proliferation, migration and invasion via the NF-κB pathway. Oncol Rep 40(2):968–978
49. Elsharawy KA et al (2020) The nucleolar-related protein dyskerin pseudouridine synthase 1 (DKC1) predicts poor prognosis in breast cancer. Br J Cancer 123(10):1543–1552
50. Ma Q et al (2022) CircARID1A binds to IGF2BP3 in gastric cancer and promotes cancer proliferation by forming a circARID1A-IGF2BP3-SLC7A5 RNA-protein ternary complex. J Exp Clin Cancer Res 41(1):251
51. Chen Q et al (2022) Circular RNA ACTN4 promotes intrahepatic cholangiocarcinoma progression by recruiting YBX1 to initiate FZD7 transcription. J Hepatol 76(1):135–147